

Article

Temporal and Spatial Analysis of PM_{2.5} and O₃ Pollution Characteristics and Transmission in Central Liaoning Urban Agglomeration from 2015 to 2020

Ju Wang *, Yue Zhong, Zhuoqiong Li and Chunsheng Fang

College of New Energy and Environment, Jilin University, Changchun 130012, China; zhongyue20@mails.jlu.edu.cn (Y.Z.); zhuoqiong21@mails.jlu.edu.cn (Z.L.); fangcs@jlu.edu.cn (C.F.)
* Correspondence: wangju@jlu.edu.cn

Abstract: The central Liaoning urban agglomeration is an important heavy industry development base in China, and also an important part of the economy in northeast China. The atmospheric environmental problems caused by the development of heavy industry are particularly prominent. Trajectory clustering, potential source contribution (PSCF), and concentration weighted trajectory (CWT) analysis are used to discuss the temporal and spatial pollution characteristics of PM_{2.5} and ozone concentrations and reveal the regional atmospheric transmission pattern in central Liaoning urban agglomeration from 2015 to 2020. The results show that: (1) PM_{2.5} in the central Liaoning urban agglomeration showed a decreasing trend from 2015 to 2020. The concentration of PM_{2.5} is the lowest in 2018. Except for Benxi (34.7 µg/m³), the concentrations of PM_{2.5} in other cities do not meet the standard in 2020. The ozone concentration in Anshan, Liaoyang, and Shenyang reached the peaks in 2017, which are 68.76 µg/m³, 66.27 µg/m³, and 63.46 µg/m³ respectively. PM_{2.5} pollution is the highest in winter and the lowest in summer. The daily variation distribution of PM_{2.5} concentration showed a bimodal pattern. Ozone pollution is the most serious in summer, with the concentration of ozone reaching 131.14 µg/m³ in Shenyang. Fushun is affected by Shenyang intercity pollution, and the ozone concentration is high. (2) In terms of spatial distribution, the high values of PM_{2.5} are concentrated in monitoring stations in urban areas. On the contrary, the concentration of ozone in suburban stations is higher. The high concentration of ozone in the northeast of Anshan, Liaoyang, Shenyang to Tieling, and Fushun extended in a band distribution. (3) Through cluster analysis, it is found that PM_{2.5} and ozone in Shenyang are mainly affected by short-distance transport airflow. In winter, the weighted PSCF high-value area of PM_{2.5} presents as a potential contribution source zone of the northeast trend with wide coverage, in which the contribution value of the weighted CWT in the middle of Heilongjiang is the highest. The main potential source areas of ozone mass concentration in spring and summer are coastal cities and the Bohai Sea and the Yellow Sea. We conclude that the regional transmission of pollutants is an important factor of pollution, so we should pay attention to the supply of industrial sources and marine sources of marine pollution in the surrounding areas of cities, and strengthen the joint prevention and control of air pollution among regions. The research results of this article provide a useful reference for the central Liaoning urban agglomeration to improve air quality.

Keywords: PM_{2.5}; O₃; transmission pathways; backward trajectory; PSCF; CWT



Citation: Wang, J.; Zhong, Y.; Li, Z.; Fang, C. Temporal and Spatial Analysis of PM_{2.5} and O₃ Pollution Characteristics and Transmission in Central Liaoning Urban Agglomeration from 2015 to 2020. *Sustainability* **2022**, *14*, 511. <https://doi.org/10.3390/su14010511>

Academic Editors: Weixin Yang, Hone-Jay Chu, Guanghui Yuan and Yunpeng Yang

Received: 22 October 2021

Accepted: 27 December 2021

Published: 4 January 2022

Publisher's Note: MDPI stays neutral with regard to jurisdictional claims in published maps and institutional affiliations.



Copyright: © 2022 by the authors. Licensee MDPI, Basel, Switzerland. This article is an open access article distributed under the terms and conditions of the Creative Commons Attribution (CC BY) license (<https://creativecommons.org/licenses/by/4.0/>).

1. Introduction

With the rapid development of the social economy, air pollution has become an increasingly serious environmental problem. Epidemiological studies have found that long-term exposure to air pollution will increase the risk of disease. For example, fine particulate matter (PM_{2.5}) is significantly associated with an increase in the prevalence of diabetes; short-term exposure to high concentrations of PM_{2.5} and ozone (O₃) will increase cardiovascular disease, respiratory disease, and non-risk of accidental death [1–3]. Since 2013,

regional atmospheric environmental problems mainly characterized by PM_{2.5} pollution have attracted widespread attention in China. Therefore, China has formulated and issued a series of policies to alleviate air pollution. From 2015 to 2020, PM_{2.5} pollution in China has been significantly reduced, while ozone pollution has become increasingly serious [4–9].

Central Liaoning Urban Agglomeration (CLUA) is located in the Northeast Plain. Due to the concentrated urban distribution, dense population, and industrial structure dominated by heavy industry, air pollution is serious. In 2020, the proportion of PM_{2.5} and O₃ as the primary pollutants in Liaoning Province in the days exceeding the standard was 62.9% and 33.8% respectively. The annual average concentration of PM_{2.5} was 38 µg/m³ which exceeds the secondary standard of ambient air quality [10]. The air quality of Central Liaoning Urban Agglomeration may be affected by regional anthropogenic emissions. In winter, the transboundary pollution of PM_{2.5} is extremely significant. Some studies also found that there was regional transmission of pollutants in Central Liaoning Urban Agglomeration and Harbin-Changchun urban agglomeration [11,12]. Straw burning and coal-burning heating during winter resulted in heavy PM_{2.5} pollution, and the interannual change of PM_{2.5} in Northeast China showed an obvious upward trend from 1998 to 2016. MDA8 (maximum daily 8 h average) O₃ increased and the number of days exceeding the standard continued to increase which can be attributed to the superimposed effects of atmospheric long-distance transport and anthropogenic emissions [13–17].

Many studies have mentioned the occurrence of air pollution in various urban agglomerations, such as the Beijing-Tianjin-Hebei region, Harbin-Changchun region, Yangtze River Delta, etc., while there are few studies on Northeast China and Central Liaoning Urban Agglomerations [18–20]. This study collected PM_{2.5} and O₃ concentration data in CLUA (Anshan, Benxi, Fushun, Liaoyang, Shenyang, and Tieling) from 2015 to 2020 and analyzed its temporal and spatial characteristics to determine the level of pollutants. Specifically, the aim was to (1) study the long-term temporal and spatial changes of the mass concentrations of PM_{2.5} and O₃ and (2), through the back trajectory HYSPLIT model and cluster analysis, discuss the regional transportation of PM_{2.5} and ozone in Shenyang, which is the center of Central Liaoning Urban Agglomeration, in order to provide a useful reference for CLUA to improve air quality.

2. Data Sources and Methods

2.1. Data Sources

The geographical location of the study area is shown in Figure 1. This study used in situ data from a total of 38 air quality monitoring stations (Table 1) in six cities in central Liaoning urban agglomeration from 2015 to 2020 (<http://www.cnemc.cn/> accessed on 14 May 2021). Among them, O₃ data used ozone eight-hour moving average (O₃-8 h), and PM_{2.5} used hourly monitoring data. Ozone is measured by UV spectrophotometry (Thermo Scientific Model 49iQ Ozone Analyzer). PM_{2.5} is passed β X-ray absorption method and light scattering method were used for real-time determination (Thermo Scientific Model 5030i Sharp Particulate Monitor). The season division refers to the meteorological industry-standard “Climate Season Division” (QX/T152-2012) and the annual difference is adjusted. The results are: spring (1 April–31 May), summer (1 June–31 August), autumn (1 September–31 October), winter (1 November–31 March of the following year).

2.2. Research Method

The Geographical Information System (GIS)-TrajStat software is used for backward trajectory clustering, potential source contribution analysis, and concentration weighted trajectory analysis, and grids were divided by 1° × 1° within the trajectory range [21,22].

2.2.1. Cluster Analysis

The Hybrid Single Particle Lagrangian Integrated Trajectory (HYSPLIT) model (<http://ready.arl.noaa.gov/HYSPLIT.php> accessed on 12 July 2021) developed by the National Oceanic and Atmospheric Administration (NOAA) was used to simulate 72 h

backward trajectories at 100 m altitude for Shenyang to analyze atmospheric pollutant transportation [23,24].

In the study, to understand the regional transport processes effects, we used $1^\circ \times 1^\circ$ Global Data Assimilation System (GDAS) data from National Centers for Environmental Prediction (NCEP). We also calculated the 72 h backward airflow trajectory at 0:00, 6:00, 12:00, and 18:00 every day from 2015 to 2020. Euclidean classification method is used to analyze the transport path of regional air mass through data statistics of various trajectories after clustering, which can distinguish trajectories with similar directions but large difference in length [25]. Then we could better distinguish the contribution of long-distance and short-distance transmissions from different directions.

Table 1. The details of 38 air quality monitoring stations.

Cities	Air Quality Monitoring Sites			
	Name	Abbr.	Longitude (°E)	Latitude (°N)
Anshan	MingDa New District	MD	123.1289	41.0228
	QianShan Mountain	QS	123.0156	41.0831
	ShenGouSi	SG	123.044	41.1196
	TaiPing	TP	123.0485	41.1442
	TieXi District Industrial Park	TD	122.9481	41.0833
	Tiexi Sandao Street	TSS	122.9642	41.0971
	TaiYang Cheng	TYC	123.011	41.0931
Benxi	Cai Tun	CT	123.7308	41.3047
	Da Yu	DY	123.8436	41.3283
	Dong Ming	DM	123.7669	41.2864
	Wei Ning	WN	123.8142	41.3472
	Xi Lake	XL	123.7528	41.3369
	Xinli Tun	XT	123.7989	41.2692
Fushun	DaHuoFang Reservoir	DHF	124.0878	41.8864
	DongZhou District	DZ	124.0383	41.8625
	ShenFuXinCheng	SF	123.7117	41.8417
	ShunCheng District	AC	123.9169	41.8828
	WangHua District	WH	123.81	41.8469
	XinFu District	XF	123.9	41.8594
Liaoyang	BinHe Road	BH	123.1761	41.2736
	HongWei District	HW	123.2	41.1953
	TieXi District industrial park	TXD	123.1417	41.2894
	XinHua Yuan	XY	123.15	41.2553
Shenyang	CangHai Road	CH	123.284	41.7694
	LingDong Street	LD	123.428	41.8472
	DongLing Road	DL	123.542	41.8336
	JingShen Street	JS	123.3783	41.9228
	TaiYuan Street	TY	123.3997	41.7972
	YuNong Road	YN	123.5953	41.9086
	WenHua Road	WH	123.41	41.765
	XiaoHeYan Road	XHY	123.478	41.7775
	SenLin Road	SL	123.6836	41.9339
	Eastern of HunNan Road	HN	123.535	41.7561
ShenLiaoXi Road	SLX	123.2444	41.7347	
Tieling	Western of HuiGong Street	HG	123.8139	42.3022
	Northern of JinShaJiang Road	JSJ	123.7153	42.2217
	ShuiShang Park	SP	123.8469	42.292
	Eastern of YinZhou Road	YZE	123.8489	42.2864

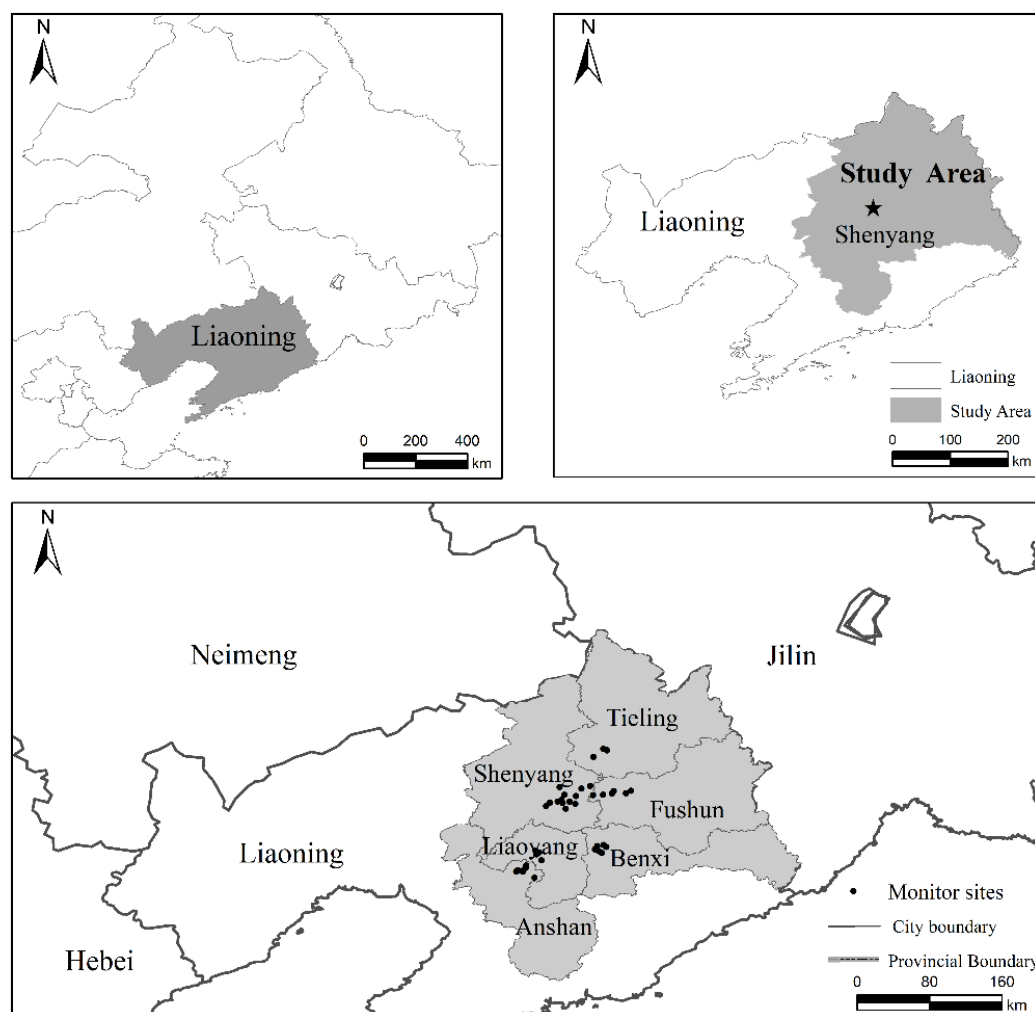


Figure 1. Air quality monitoring station in CLUA.

2.2.2. PSCF Analysis

Potential source contribution analysis (PSCF) is also called residence time analysis (RT). The ratio of the length of track l in the grid (i, j) to the length of the whole track is multiplied by the backward track 72 h, and the result is the residence time of pollutants in the grid [26]. PSCF identifies the possible pollution emission source areas by combining the air mass clustering trajectory and pollutant concentration value. PSCF function is a conditional probability function that pollutants carried by air masses passing through a unit area exceed the set pollutant threshold [27]. The PSCF value calculated by this function is the ratio of the number of pollution tracks as m_{ij} passing through the grid (i, j) in all track ranges to the number of tracks as n_{ij} passing through the grid [28]. The calculation method is shown in Equation (1).

$$PSCF_{ij} = \frac{m_{ij}}{n_{ij}} \quad (1)$$

In this paper, potential source contribution analysis (PSCF) is used to further identify the potential sources of air pollution in Shenyang [29,30], setting $PM_{2.5}$ concentration threshold of $35 \mu\text{g}/\text{m}^3$ and O_3 concentration threshold of $100 \mu\text{g}/\text{m}^3$ for all pollution trajectories, to determine the location of potential pollution sources affecting the atmospheric environment in Shenyang. However, in order to reduce the uncertainty of PSCF value, the weight factor W_{ij} is introduced and called WPSCF [31], such as Equations (2) and (3).

$$W_{ij} = \begin{cases} 1.00 & (80 < n_{ij}) \\ 0.70 & (25 < n_{ij} \leq 80) \\ 0.42 & (15 < n_{ij} \leq 25) \\ 0.17 & (n_{ij} \leq 15) \end{cases} \quad (2)$$

$$WPSCF_{ij} = \frac{m_{ij}}{n_{ij}} W_{ij} \quad (3)$$

where m_{ij} is the number of pollution tracks passing through the grid (i, j) ; n_{ij} is the total number of tracks passed.

2.2.3. CWT Analysis

The values calculated by the PSCF method are the same when the pollutant concentrations of the trajectories are only slightly higher or much higher than the standard [32,33]. As a result, it may be difficult to distinguish between moderate and strong sources by PSCF method. Therefore, in this paper, the concentration-weighted trajectory (CWT) analysis method is used to calculate the average weighted concentration of each trajectory, which reveals the contribution of different regions to the air pollution in Shenyang by setting the mesh precision of CWT to be the same as that of PSCF [34,35]. The same weight factor W_{ij} from the PSCF method is introduced to distinguish the source intensity of potential sources, which is called the weighted average concentration value (WCWT value), as shown in Equation (4).

$$C_{ij} = \frac{W_{ij}}{\sum_{l=1}^M \tau_{ijl}} \sum_{l=1}^M C_l \tau_{ijl} \quad (4)$$

where C_{ij} is the average weight concentration in the grid (i, j) , l is the index of the track, C_l is the pollutant concentration measured when track l arrives, M is the total number of tracks, and τ_{ijl} is the time that the trajectory l stays in the mesh (i, j) . The higher the value of C_{ij} , the greater the contribution of the trajectory to the air pollution in Shenyang.

3. Results and Discussion

3.1. Temporal Variation

The annual average concentrations and change trends of $PM_{2.5}$ and O_3 in six cities of CLUA are investigated as shown in Figure 2. $PM_{2.5}$ basically showed a trend of declining from 2015 to 2020. The average concentration of $PM_{2.5}$ in Fushun decreased by 18% from 2015 to 2016, and increased slightly in 2017 and 2019, but was still lower than $53 \mu\text{g}/\text{m}^3$ in 2015. China began to implement the environmental protection tax law in 2018 to strengthen the management of air pollution punishment, which explains why the $PM_{2.5}$ concentration in each city was the lowest in 2018. In addition, straw burning was prohibited in the study area, and Liaoning Province began to completely ban small coal-fired boilers of 10 tons and below in 2016 to improve air quality. The average concentration of $PM_{2.5}$ in Anshan City decreased from $67 \mu\text{g}/\text{m}^3$ to $41.6 \mu\text{g}/\text{m}^3$, which was 66.4% lower in 2020 than in 2015. In 2020, the lowest $PM_{2.5}$ value appeared in Benxi City, which was $34.7 \mu\text{g}/\text{m}^3$. Except for Benxi, $PM_{2.5}$ in other cities (Anshan, Fushun, Liaoyang, Shenyang, Tieling) did not meet China Class II Environmental Air Quality Standard (CAAQS) limited to $35 \mu\text{g}/\text{m}^3$. This shows that the government needs to strengthen particulate matter control in these cities. Unlike $PM_{2.5}$, the annual average concentration of ozone does not change much in various regions, and the trend of change is slightly different. This can be attributed to the fact that ozone is affected by more meteorological conditions and chemical reactions [36,37], so its regional characteristics are less obvious. The average concentration of O_3 in Shenyang increased from 2015 to 2017 and decreased significantly after reaching peak value in 2017. Among them, the ozone concentration in Anshan, Liaoyang, and Shenyang reached the peak concentrations in 2017, which were $68.76 \mu\text{g}/\text{m}^3$, $66.27 \mu\text{g}/\text{m}^3$, and $63.46 \mu\text{g}/\text{m}^3$ respectively.

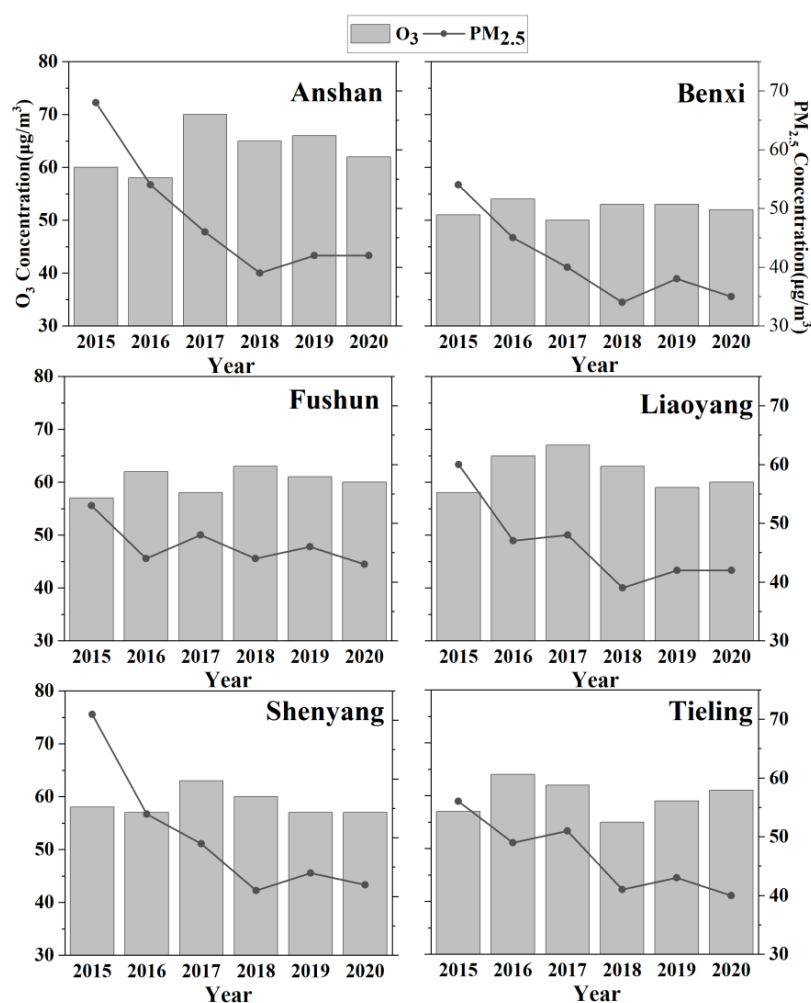


Figure 2. Inter-annual changes of PM_{2.5} and O₃ years in CLUA from 2015 to 2020.

Figure 3 shows the monthly variation of the 24-h multi-year average concentration of PM_{2.5} in CLUA from 2015 to 2020. It can be found that PM_{2.5} pollution is the most serious at the beginning and the end of the year (January to March and October to December), and the PM_{2.5} pollution is lower from May to September. In Northeast China, there is a large area of open burning of crop residues, which is one of the reasons for PM_{2.5} pollution in autumn and winter. In addition, PM_{2.5} pollution peaked in the heating period. Due to the long heating period, PM_{2.5} pollution continued until the next spring. It can be seen that the frequency of low PM_{2.5} concentration in Benxi area is higher, which also indicates that the PM_{2.5} pollution in Benxi is relatively lower than in other areas, because Benxi is rainy in summer and autumn, and the wind direction is southeast, which is conducive to the diffusion of pollutants. In general, the PM_{2.5} concentration in several cities resulted in high values at night and low values during the day. In this latter case, low-concentration PM_{2.5} were registered from 14:00 to 17:00, while the peak of PM_{2.5} mainly were registered from 7:00 to 9:00 and from 18:00 to 23:00. The first peak is related to atmospheric stability and the increase of human activities during this period [38]. This can be attributed to the intensification of atmospheric turbulence and the gradual decrease of PM_{2.5} concentration with the increase of temperature in the morning. The evening peak in the cities appears after sunset, so the PM_{2.5} emission increases. In addition, the surface radiation cooling reduces the height of the boundary layer, and the atmosphere tends to be stable, leading PM_{2.5} concentration to continue to rise [39].

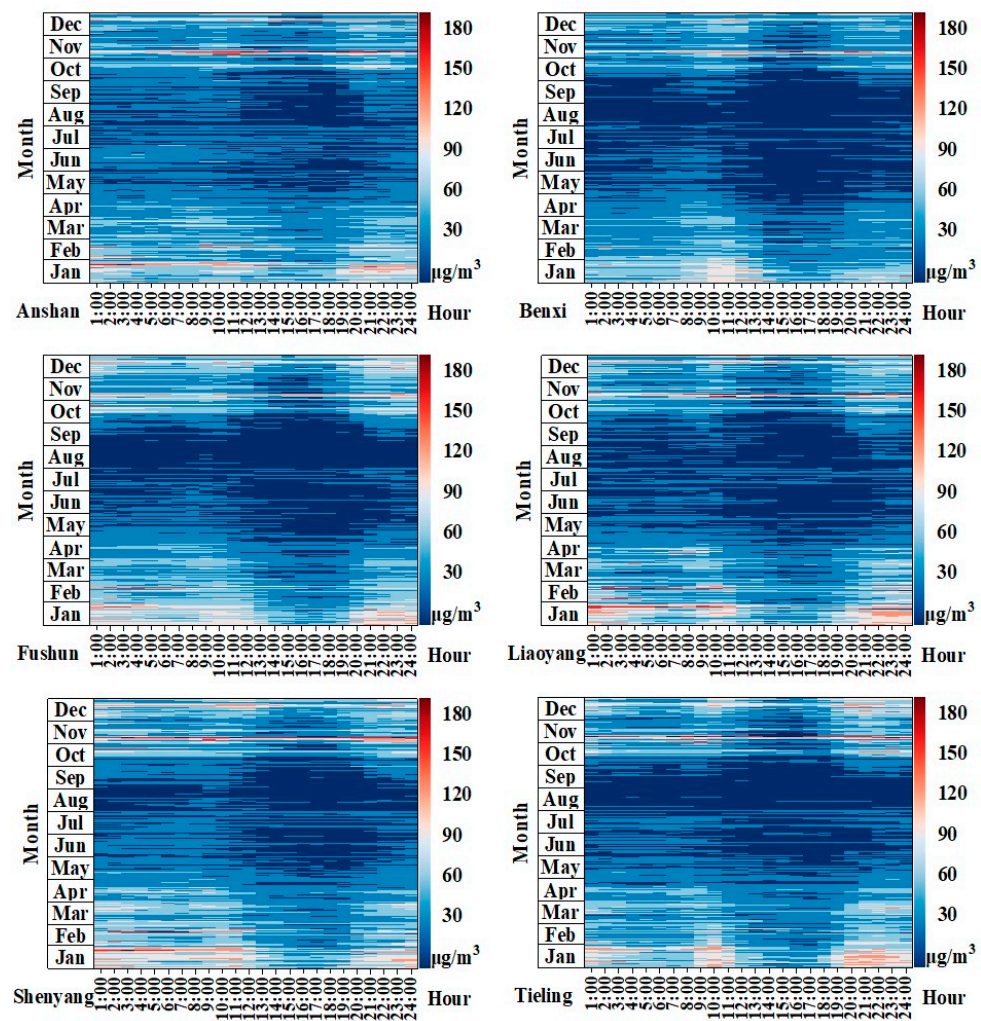


Figure 3. Hourly variation of multi-year average concentration of PM_{2.5} in different months in CLUA from 2015 to 2020.

Figures 4 and 5 are box charts of daily average concentrations of PM_{2.5} and O₃ in different seasons in CLUA from 2015 to 2020 respectively. The upper and lower frames of the box represent 75% and 25% quantiles respectively. The data points next to the box in the figures correspond to the daily average concentration of pollutants, and a normal distribution curve is added according to the concentration value. It is obvious that PM_{2.5} pollution trends are the same in all cities. PM_{2.5} pollution is the most serious in winter, followed by spring and autumn, and significantly lower in summer than in other seasons. In summer, the concentration of PM_{2.5} in the Anshan area is the highest, 32.02 µg/m³ (<35 µg/m³). However, the concentration of PM_{2.5} in other cities does not exceed 30 µg/m³. It may be related to the fact that Anshan is a heavy industrial city and the main pollution source is a fixed source. Compared with other seasons, the rainy weather in summer has an obvious effect on the wet deposition of pollutants, so the PM_{2.5} concentration is relatively lower [40]. In spring and autumn, PM_{2.5} pollution is the most serious in Shenyang, followed by Tieling and Anshan. The concentration of PM_{2.5} in Benxi is the lowest. In winter, PM_{2.5} pollution in Shenyang is the most serious (69.57 µg/m³), which is 2.46 times higher than that in summer. The concentration of PM_{2.5} in Benxi City is the lowest, 57.9 µg/m³. This is consistent with other results obtained using MODIS inversion data [41,42]. The high concentration in winter is mainly due to the high population density in the built-up area and the low temperature in winter in the north, so the amount of coal combustion increases. In addition, inversion is more likely to occur in winter, which is not conducive to the diffusion of pollutants [43,44].

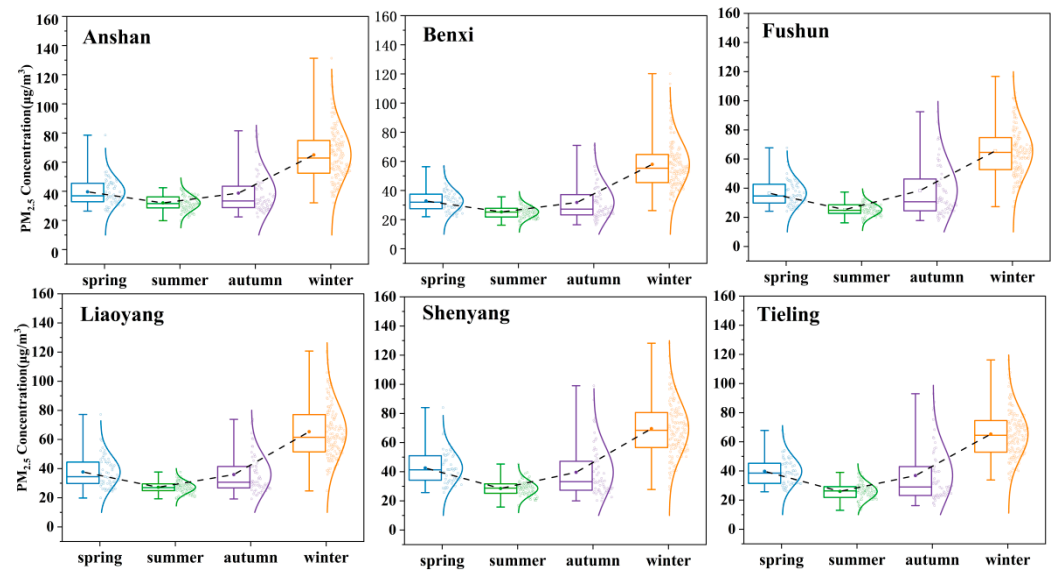


Figure 4. Seasonal variation of $PM_{2.5}$ in CLUA from 2015 to 2020.

Being affected by the seasonal variation of meteorological conditions, the ozone concentration is opposite to that of $PM_{2.5}$. In spring and summer, it is significantly higher than that in autumn and winter. The seasonal pattern of ozone in central Liaoning urban agglomeration is the same as that in other regions, with the overall pattern as summer > spring > autumn > winter [45–47]. In summer, the O_3 concentration in Shenyang is $131.14 \mu\text{g}/\text{m}^3$, and the O_3 concentration in Benxi is $95.3 \mu\text{g}/\text{m}^3$. Some studies have shown that direct emission of surface ozone is different from that of other air pollutants. O_3 is mainly generated by nitrogen oxides (NO_x) and volatile organic compounds (VOCs) through a series of complex photochemical reactions [48,49]. The high temperature and high chemical reaction rate in spring and summer make the ozone concentration much higher than that in other seasons. In addition, Benxi is different from other regions, and ozone concentration in summer is lower than that in spring. The ozone concentration in Fushun is higher in six cities. Huang et al. mentioned that there is intercity pollution between Fushun and Shenyang. Therefore, the ozone concentration in the monitoring stations near Shenyang is higher (Figure 6).

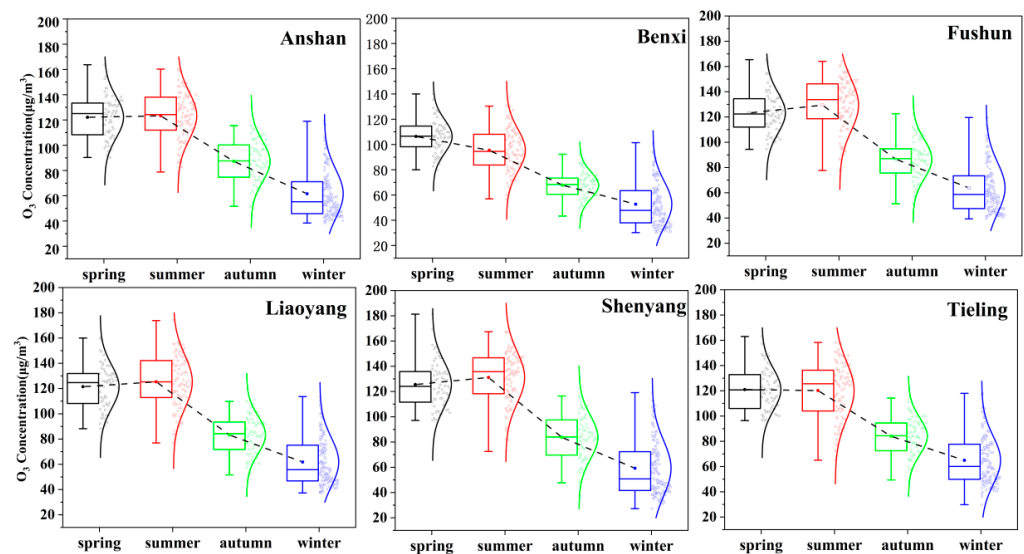


Figure 5. Seasonal variation of O_3 in CLUA from 2015 to 2020.

3.2. Spatial Analysis

The spatial sites distribution of O_3 and $PM_{2.5}$ in CLUA is shown in Figures 6 and 7. $PM_{2.5}$ and O_3 of all monitoring stations in Shenyang showed an obvious downward trend from 2015 to 2020. In 2015, the high concentrations of $PM_{2.5}$ were mainly located in LD, TY, SLX in Shenyang, TD, and TSS in Anshan. On the whole, since 2016, the concentration values of monitoring stations near the junction of Shenyang and Fushun have been higher. The stations with high concentrations of $PM_{2.5}$ are mainly concentrated in Shenyang urban areas, TD, SF, and WH. These stations are mostly concentrated in urban areas with high population, which leads to a higher concentration of pollutants caused by motor vehicles and industrial discharge.

The spatial distribution trend of ozone is basically the opposite of $PM_{2.5}$. The concentration of O_3 in rural areas is higher, such as XT, DY, DM, HW, and JSJ, etc. As a secondary pollutant, the formation of surface ozone is mainly related to its precursors (NO_x and VOCs). The source analysis of atmospheric VOCs in some areas shows that the contribution rate of motor vehicle sources is high, which is the main source of urban atmospheric VOCs [50,51]. The ozone pollution occurring in the urban areas is transported to the suburbs with certain meteorological conditions [52]. The higher vegetation coverage is conducive to photochemical reaction, resulting in higher ozone concentration in the suburbs [53]. In addition, it can be found that the O_3 concentration is higher at the stations near the junction of Liaoyang and Anshan. From 2015 to 2020, the O_3 concentration in western cities are lower than that in eastern cities. The high ozone concentration is distributed in a belt from Anshan, Liaoyang and Shenyang to Tieling and Fushun in the northeast. While the ozone concentration of Benxi in the east is always low, which is consistent with the results in Figure 2. Figure 8 shows that the ozone concentration in CLUA increased significantly from 2015 to 2017, and began to decrease gradually in 2018. It shows that while dealing with climate change, controlling pollutant emission reduction plays an active role in ozone mass concentration control.

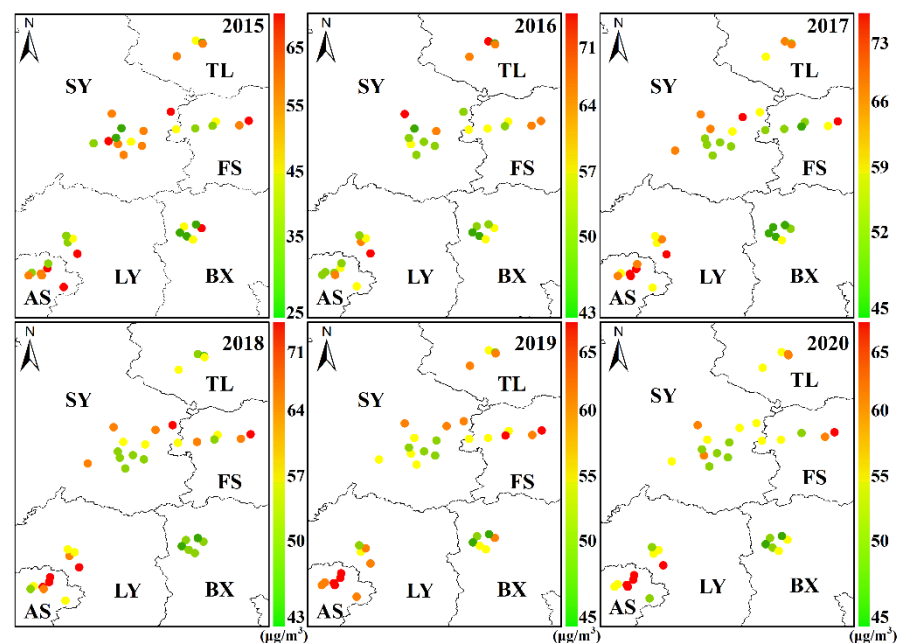


Figure 6. Spatial site distribution of annual average mass concentration of MDA8 O_3 in CLUA $PM_{2.5}$ annual average mass concentration of CLUA from 2015 to 2020 (AS: Anshan; BX: Benxi; FS: Fushun; LY: Liaoyang; SY: Shenyang; TL: Tieling).

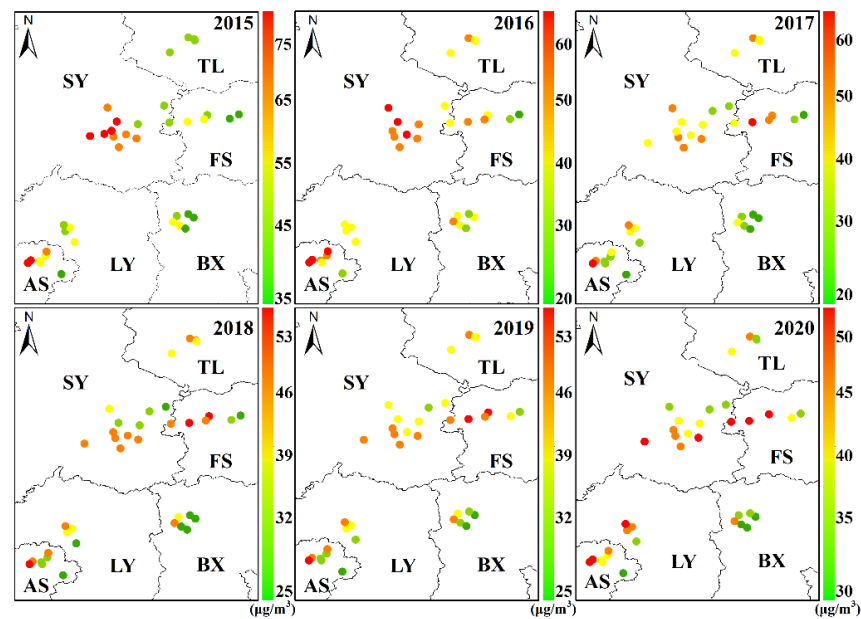


Figure 7. Spatial site distribution of $PM_{2.5}$ annual average mass concentration in CLUA from 2015 to 2020 (AS: Anshan; BX: Benxi; FS: Fushun; LY: Liaoyang; SY: Shenyang; TL: Tieling).

3.3. Transmission Path Characteristics in Shenyang Region

As the Shenyang area is the geographical and economic center of CLUA, its $PM_{2.5}$ and O_3 pollution is severe. Therefore, this study selects Shenyang city for backward trajectory cluster analysis and potential source area analysis. Cluster analysis of the backward airflow trajectories transported to Shenyang at 0:00, 6:00, 12:00, and 18:00 every day from 2015 to 2020 (Figure 9). There are six categories of backward trajectories in spring. The air flows in spring are mainly south (trajectory 1 and trajectory 5) and northwest (trajectory 3 and trajectory 6), which account for 67.79% of the airflows in spring. There are four categories of backward trajectories in summer. In summer, affected by the marine airflows, the southerly airflows (trajectory 1) and southeast airflows (trajectory 4) are predominant, accounting for 68.43% of the airflows in summer. There are seven categories of backward trajectories in autumn and six categories of backward trajectories in winter. In autumn and winter, the airflows are mostly northwest and the transmission distance is longer with faster speed, which may be related to the propagation of the East Asian winter monsoon. Except in summer, the airflows from the Beijing-Tianjin-Hebei region have all turned back significantly.

Based on the cluster analysis results of airflow backward trajectories in each season, the $PM_{2.5}$ and ozone concentration data in Shenyang are combined (Table 2) to quantitatively analyze the impact of various trajectories on $PM_{2.5}$ and ozone in Shenyang.

Consistent with the results discussed above, the $PM_{2.5}$ concentration corresponding to each air flow in autumn and winter is higher than that in spring and summer. In winter, the $PM_{2.5}$ concentration corresponding to the air flow (trajectory 3) from the junction of Liaoning and Hebei, Bohai Bay and southwest Liaoning is the highest, $106.02 \mu\text{g}/\text{m}^3$. The second is the air flow from Northeast Inner Mongolia, northwest Jilin and northeast Liaoning (trajectory 6), and the corresponding $PM_{2.5}$ concentration is $105.23 \mu\text{g}/\text{m}^3$. The corresponding concentration of ozone in the southerly flow (trajectory 1) from the Yellow Sea in spring is $142.41 \mu\text{g}/\text{m}^3$, followed by the air flow (trajectory 5) is $136.5 \mu\text{g}/\text{m}^3$.

The long-distance transport of northwest air flow from Hunshandak Sandy Land in Northwest Inner Mongolia and the Gobi Desert in central Mongolia is the main transport path affecting the $PM_{2.5}$ concentration in Shenyang in four seasons. In addition, southwest air flows through densely populated areas such as Beijing, Tianjin, and Hebei. The Bohai Sea has heavy shipping emissions, making it another main transmission path affecting $PM_{2.5}$ pollution in Shenyang.

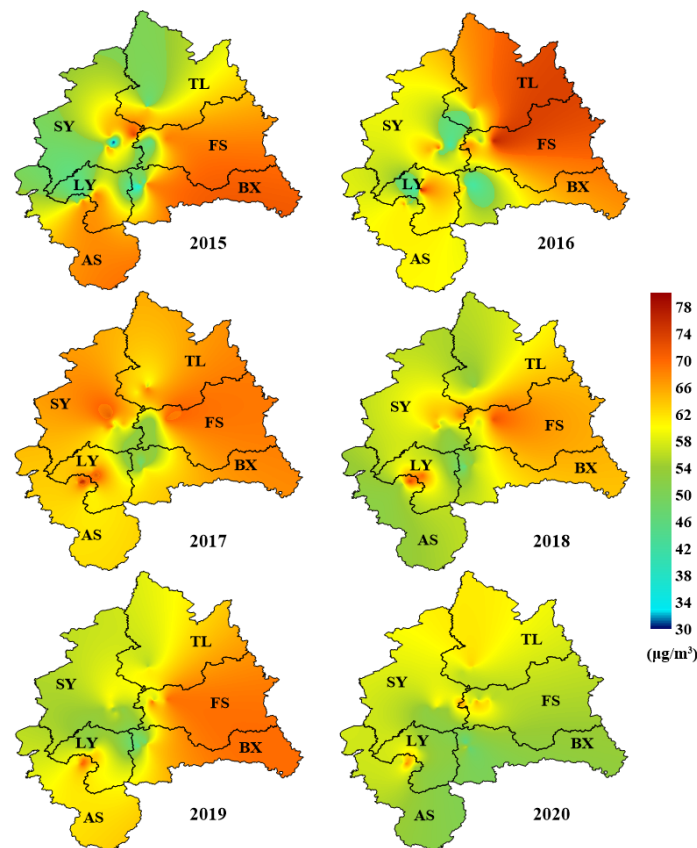


Figure 8. Spatial distribution of annual average mass concentration of MDA8 O₃ in CLUA from 2015 to 2020 (AS: Anshan; BX: Benxi; FS: Fushun; LY: Liaoyang; SY: Shenyang; TL: Tieling).

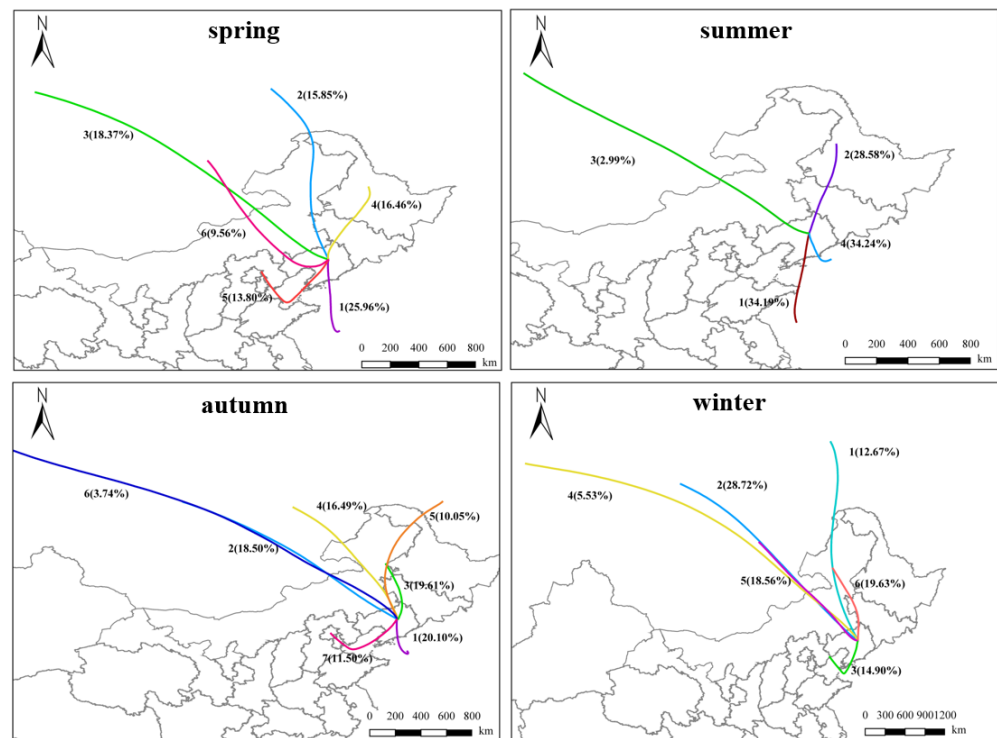


Figure 9. Clustering analysis of backward trajectories of each season in Shenyang from 2015 to 2020 (the trajectories are marked with number and frequency).

Table 2. Statistical results of the mass concentration of all kinds of air flow in the four seasons of Shenyang.

Season	Air Mass Type	PM _{2.5}	Stdev	Number	Ozone	Stdev	Number
spring	1	60.51	24.70	202	142.41	32.84	189
	2	60.64	28.59	65	111.46	7.57	14
	3	59.25	23.82	100	118.87	15.45	26
	4	69.00	34.10	124	128.95	21.41	50
	5	67.13	28.36	138	136.50	26.83	114
	6	68.01	31.71	79	126.39	20.51	31
summer	1	50.13	13.82	286	137.58	31.06	301
	2	48.56	11.93	87	126.94	21.51	113
	3	58.19	23.81	9	125.66	22.24	8
	4	49.32	13.65	224	139.83	32.71	230
autumn	1	72.59	38.98	144	119.96	15.78	11
	2	57.67	20.13	76	126.97	19.32	5
	3	70.91	30.63	117	127.91	20.74	37
	4	72.21	59.55	93	113.84	13.10	6
	5	63.65	48.37	22	0.00	0.00	0
	6	58.04	20.42	5	125.80	0.00	1
	7	59.25	25.67	150	121.29	21.59	44
winter	1	78.52	57.48	543	112.41	15.37	4
	2	90.24	65.41	506	109.51	5.96	10
	3	106.02	85.85	614	114.84	11.12	16
	4	66.15	33.99	45	0.00	0.00	0
	5	76.45	41.05	222	111.22	5.83	4
	6	105.23	54.45	489	120.49	19.19	50

3.4. Characteristics of Potential Source Areas in Shenyang

We conduct the potential source contribution factor (WPSCF) analysis and the concentration weight trajectory (WCWT) analysis based on the backward trajectory of each season in Shenyang from 2015 to 2020, in order to fully reflect the long-term impact characteristics and contribution of potential source regions on the mass concentration of PM_{2.5} and O₃ in Shenyang. The results are shown in Figures 10–13. The larger the calculated value of WPSCF, the greater the impact of the area on the mass concentration of PM_{2.5} and O₃ in Shenyang. The higher value of WCWT, the greater the contribution of the grid area to the pollution of PM_{2.5} and O₃ in Shenyang.

The WPSCF value of PM_{2.5} is the lowest in summer, and it can be found that WPSCF and WCWT have consistent spatial distribution characteristics in central Shandong. It can be seen that the regions with a higher contribution to the PM_{2.5} concentration in Shenyang in spring were concentrated in the central Shandong Province and the northwestern parts of Jiangsu Province, with WPSCF value higher than 0.7 and corresponding WCWT value higher than 50 µg/m³ (Figures 10 and 12). In summer, WPSCF value is higher near Zaozhuang and Jinan in Shandong Province, and WCWT value is 45~50 µg/m³. The regions with relatively high WPSCF in autumn are mainly concentrated in Beijing-Tianjin-Hebei Urban Agglomeration and northwestern part of the Shandong Province, and the WCWT value is higher than 80 µg/m³. In winter, due to the heavy PM_{2.5} pollution, the WPSCF value of PM_{2.5} is high and wide, indicating that the PM_{2.5} pollution in Shenyang has certain regional characteristics. The high value of WPSCF mainly occurs in Beijing Tianjin Hebei Urban Agglomeration, Bohai Sea area, Lianyungang City, Shandong Province and Jiangsu Province, the northeast of Liaoning, the middle of Jilin, and the middle of Heilongjiang, showing a wide coverage of northeast trending potential contribution source zone (WPSCF > 0.8). It is worth noting that in the WCWT distribution, the central Heilongjiang shows more than 240 PM_{2.5}. It also mentioned that in winter, Liaoning

Province is subject to long-distance transportation from Heilongjiang Province, resulting in serious haze pollution [54].

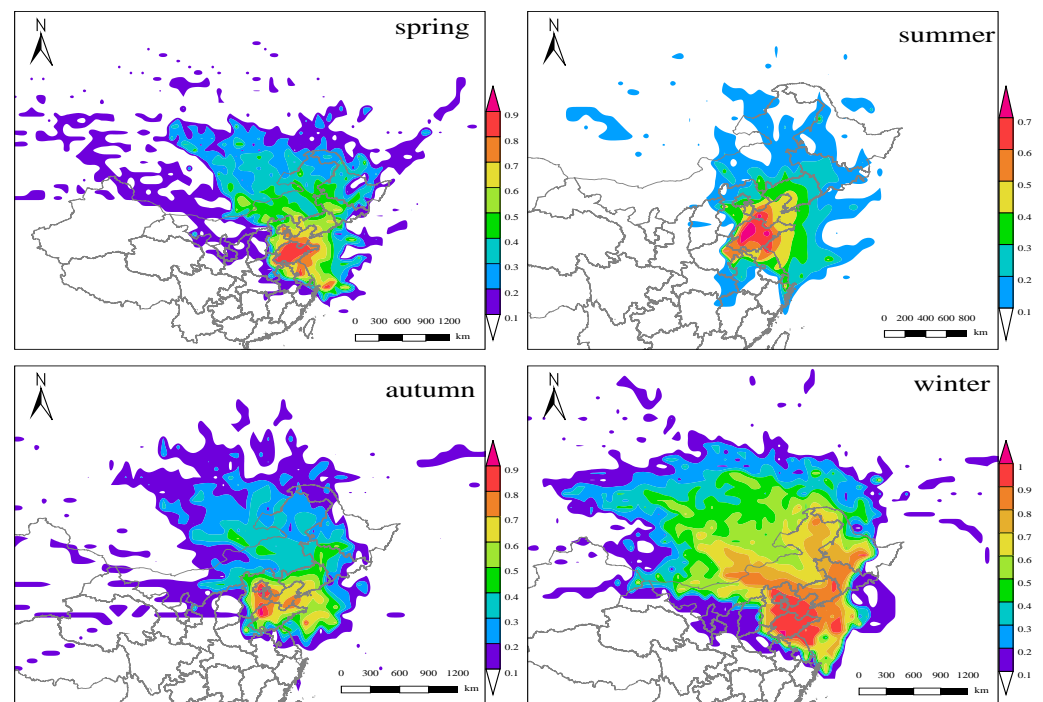


Figure 10. WPSCF distribution of $PM_{2.5}$ in Shenyang from 2015 to 2020.

It can be seen from Figure 11 that there are many regions with higher contributions of the O_3 concentration in Shenyang in spring and summer. They are mainly concentrated in Bohai Bay, Shandong Province, Jiangsu Province, and the nearby Yellow Sea. The WPSCF value is higher than 0.6 and the corresponding WCWT value is more than $110 \mu\text{g}/\text{m}^3$. Among them, Jiangsu Province is an economically developed region in China, with intensive secondary industry and serious pollutant emission. The high WPSCF values in the Bohai Sea and the Yellow Sea may be the pollutants in their adjacent areas and are transmitted to the nearby sea areas through the sea land winds. Then they are transported to the northeast along the Bohai Bay and the Yellow Sea bay, sinking in Shenyang. However, as mentioned above, compared with $PM_{2.5}$, ozone is unstable and the formation conditions are complex, so it is more difficult to determine the potential source area of ozone. PSCF and CWT methods show that the high ozone content in Shenyang mainly comes from the transmission in the Yellow Sea, Bohai Sea, and its adjacent areas.

Combined with the analysis of PSCF and CWT, it can be found that the main potential sources areas affecting the $PM_{2.5}$ mass concentration of in Shenyang in autumn and winter are Beijing-Tianjin-Hebei Urban Agglomeration, Shandong Province, Jiangsu Province, and nearby sea areas. This shows that the atmospheric circulation has an important impact on the regional transmission of the city. In addition, the main potential source areas of O_3 mass concentration in spring and summer are coastal cities and the Bohai Sea and Yellow Sea. This is also consistent with the backward air flow trajectory with heavy pollution in each season, and the influence of long-distance transmission of pollution concentration is small. Through potential source analysis, we should pay attention to the industrial source supply in the surrounding areas of cities and the marine source provided by marine pollution, and strengthen joint prevention and control of air pollution among regions.

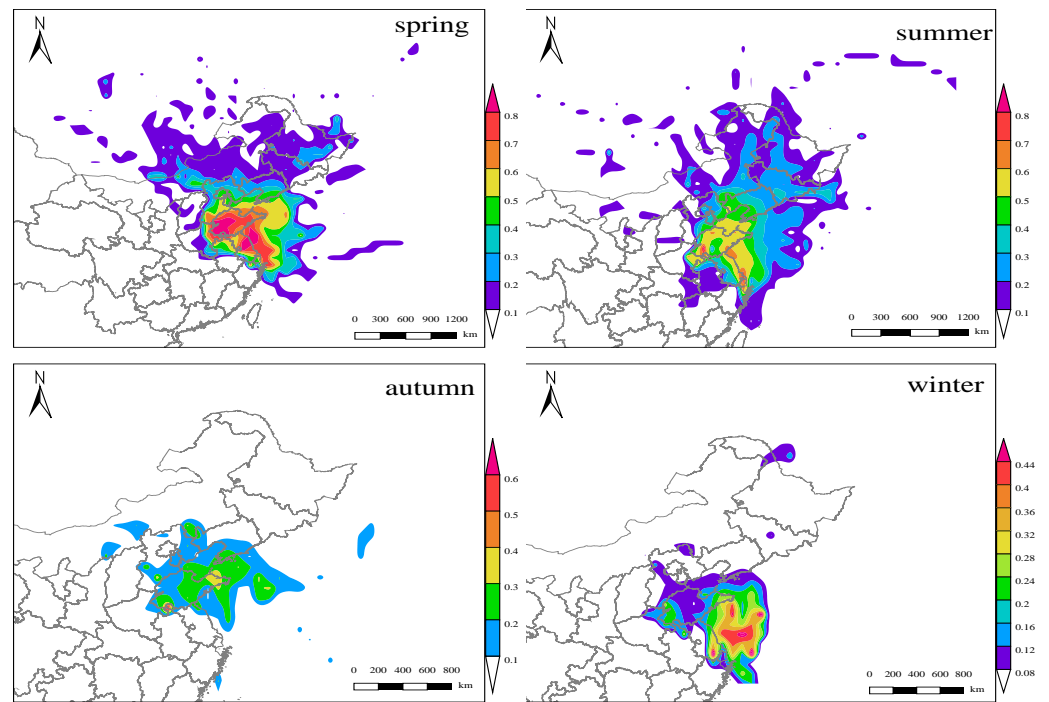


Figure 11. WPSCF distribution of O_3 in Shenyang from 2015 to 2020.

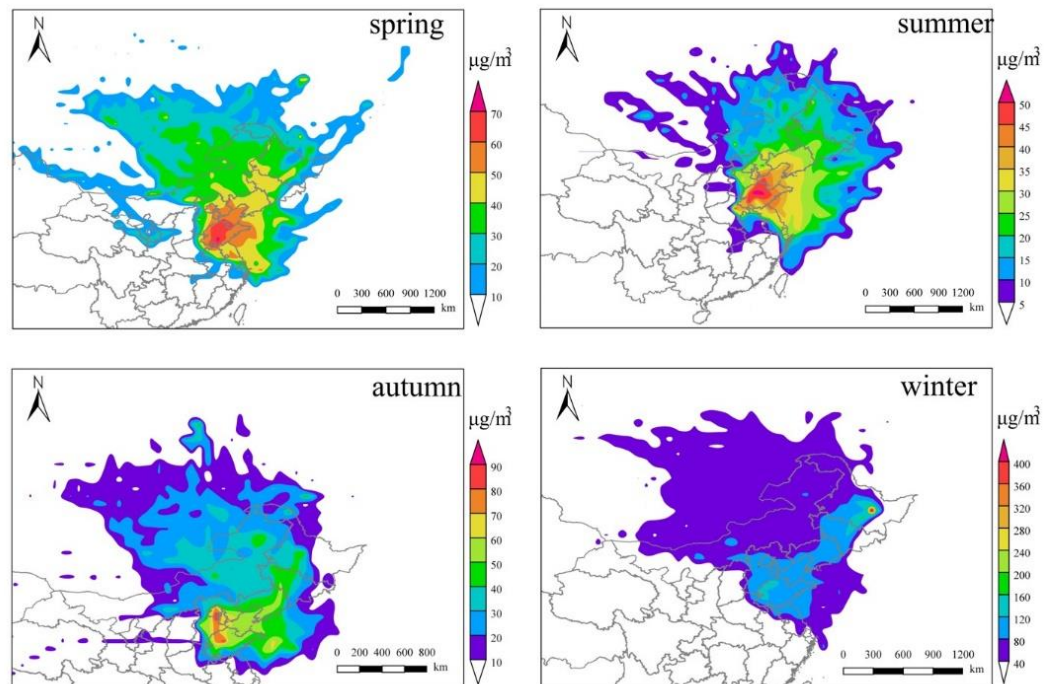


Figure 12. WCWT distribution of $PM_{2.5}$ in Shenyang from 2015 to 2020.

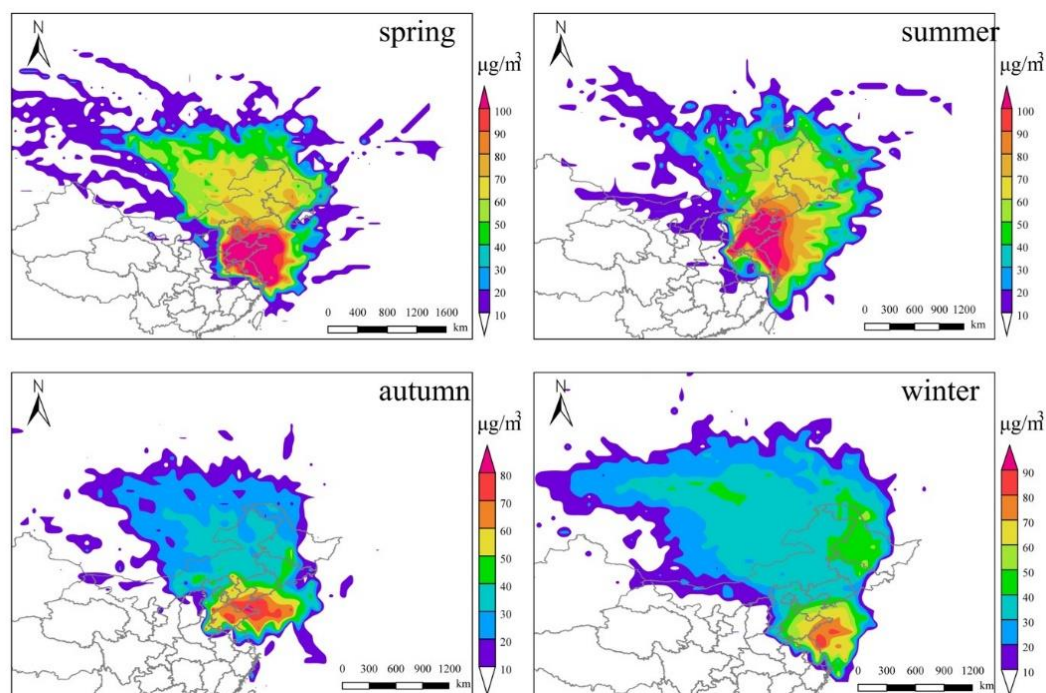


Figure 13. WCWT distribution of O₃ in Shenyang from 2015 to 2020.

4. Conclusions

The PM_{2.5} concentration has fluctuated from 2016 to 2020 in Fushun, and has declined year by year from 2015 to 2020 in other areas of the CLUA. The lowest PM_{2.5} level occurred in 2018. Except for Benxi, PM_{2.5} in other cities (Anshan, Fushun, Liaoyang, Shenyang, Tieling) did not meet the China Class II Environmental Air Quality Standard (CAAQS) limit of 35 µg/m³. The annual mean concentration of ozone has little change in different regions, and the variation trend is different. The ozone concentration in Anshan, Liaoyang, and Shenyang reached the peak value in 2017, which was 68.76 µg/m³, 66.27 µg/m³, and 63.46 µg/m³, respectively. PM_{2.5} pollution is the most severe at the beginning and the end of each year (January to March and October to December). The concentration of PM_{2.5} in all cities showed the characteristics of high at night and low during the day. Affected by human activities and atmospheric movements, there are two peaks at 7:00~9:00 and 18:00~23:00. The seasonal pattern of PM_{2.5} concentration was winter > spring > autumn > summer. In winter, PM_{2.5} pollution in Shenyang is 69.57 µg/m³, which is 2.46 times of that in summer. The seasonal pattern of ozone concentration is summer > spring > autumn > winter. In summer, The O₃ concentration in Shenyang is the highest, 131.14 µg/m³, 1.37 times of that in Benxi. The ozone concentration in Fushun area is affected by the intercity pollution in Shenyang.

In terms of the spatial distribution of PM_{2.5} and O₃ concentrations, the concentrations of PM_{2.5} in the western cities (Shenyang, Liaoyang, and Anshan) present higher than that in the eastern ones (Tieling, Fushun, and Benxi), and the higher values are concentrated in urban monitoring stations. On the contrary, the concentration of O₃ is higher in rural areas, which is related to its precursors. The high concentration of ozone in Anshan, Liaoyang, and Shenyang extends to Tieling and Fushun in the northeast. The ozone concentration of Benxi city in the east is always low. Moreover, the ozone concentration in the central Liaoning urban agglomeration began to decrease gradually in 2018.

Through backward trajectory cluster analysis, it is found that the main transmission paths affecting Shenyang are southerly short-distance and northwest long-distance airflows in spring, southerly short-distance airflow in summer, southerly and northerly airflows in autumn, and northwestern long-distance airflow in winter. In winter, southwest airflows and northeast airflows have the highest PM_{2.5} concentration, which is 106.02 µg/m³ and

105.23 $\mu\text{g}/\text{m}^3$ respectively. The ozone concentration corresponding to the southerly airflows in spring and summer is the highest, which is 142.41 $\mu\text{g}/\text{m}^3$ and 139.83 $\mu\text{g}/\text{m}^3$, respectively.

Through the WPSCF and WCWT analysis, it is found that the main potential source areas affecting the mass concentration of $\text{PM}_{2.5}$ in Shenyang in autumn and winter are Beijing-Tianjin-Hebei urban agglomeration, Shandong Province, Jiangsu Province, and nearby sea areas, showing a potential contribution source belt with a wide coverage of northeast trend. In addition, the main potential source areas of ozone mass concentration in spring and summer are mainly coastal cities and the Bohai sea and Yellow Sea. Through the analysis of potential sources, we should pay attention to the industrial source supply in the surrounding areas and the marine source provided by marine pollution. We will strengthen joint prevention and control of air pollution between regions.

Author Contributions: Conceptualization, Y.Z.; methodology, J.W.; software, Y.Z.; validation, J.W. and C.F.; formal analysis, Z.L.; investigation, Y.Z.; resources, C.F.; data curation, C.F.; writing—original draft preparation, Y.Z.; writing—review and editing, J.W., Y.Z. and C.F.; visualization, C.F.; supervision, C.F.; project administration, J.W. and C.F. All authors have read and agreed to the published version of the manuscript.

Funding: This research received no external funding.

Acknowledgments: The authors would like to thank the group members of Laboratory 537 and 142 of Jilin University.

Conflicts of Interest: The authors declare no conflict of interest.

References

1. Yang, B.Y.; Qian, Z.; Li, S.; Markevych, I.; Bloom, M.S. Ambient air pollution in relation to diabetes and glucose-homoeostasis markers in China: A cross-sectional study with findings from the 33 Communities Chinese Health Study. *Lancet Planet. Health* **2018**, *2*, e113. [[CrossRef](#)]
2. Xia, S.Y.; Huang, D.S.; Jia, H.; Zhao, Y.; Li, N.; Mao, M.Q.; Lin, H.; Li, Y.X.; He, W.; Zhao, L. Relationship between atmospheric pollutants and risk of death caused by cardiovascular and respiratory diseases and malignant tumors in Shenyang, China, from 2013 to 2016: An ecological research. *Chin. Med. J.* **2019**, *132*, 2269–2277. [[CrossRef](#)] [[PubMed](#)]
3. Lei, R.Q.; Zhu, F.R.; Cheng, H.; Liu, J.; Shen, C.W.; Zhang, C.; Xu, Y.C.; Xiao, C.C.; Li, X.R.; Zhang, J.Q.; et al. Short-term effect of $\text{PM}_{2.5}/\text{O}_3$ on non-accidental and respiratory deaths in highly polluted area of China. *Atmos. Pollut. Res.* **2019**, *10*, 1412–1419. [[CrossRef](#)]
4. Guan, Y.; Xiao, Y.; Wang, Y.M.; Zhang, N.N.; Chu, C.J. Assessing the health impacts attributable to $\text{PM}_{2.5}$ and ozone pollution in 338 Chinese cities from 2015 to 2020. *Environ. Pollut.* **2021**, *287*, 117623. [[CrossRef](#)]
5. Dong, D.X.; Xu, B.Y.; Shen, N.; He, Q. The adverse impact of air pollution on China's economic growth. *Sustainability* **2021**, *13*, 9056. [[CrossRef](#)]
6. Wu, Z.Y.; Zhang, Y.Q.; Zhang, L.M.; Huang, M.J.; Zhong, L.J.; Chen, D.H.; Wang, X.M. Trends of outdoor air pollution and the impact on premature mortality in the Pearl River Delta region of southern China during 2006–2015. *Sci. Total Environ.* **2019**, *690*, 248–260. [[CrossRef](#)] [[PubMed](#)]
7. Zhang, N.N.; Ma, F.; Qin, C.B.; Li, Y.F. Spatiotemporal trends in $\text{PM}_{2.5}$ levels from 2013 to 2017 and regional demarcations for joint prevention and control of atmospheric pollution in China. *Chemosphere* **2018**, *210*, 1176–1184. [[CrossRef](#)] [[PubMed](#)]
8. Chen, Z.; Wang, J.N.; Ma, G.X.; Zhang, Y.S. China tackles the health effects of air pollution. *Lancet* **2013**, *382*, 1959–1960. [[CrossRef](#)]
9. Guo, H.; Cheng, T.H.; Gu, X.F.; Wang, Y.; Chen, H.; Bao, F.W.; Shi, S.Y.; Xu, B.R.; Wang, W.N.; Zuo, X.; et al. Assessment of $\text{PM}_{2.5}$ concentrations and exposure throughout China using ground observations. *Sci. Total Environ.* **2017**, *601*, 1024–1030. [[CrossRef](#)]
10. Liaoning Provincial Environmental Protection Bureau. *Bulletin on the Ecological Environment of Liaoning Province in 2020*; Liaoning Provincial Environmental Protection Bureau: Shenyang, China, 2020.
11. Liu, S.C.; Xing, J.; Wang, S.X.; Ding, D.A.; Chen, L.; Hao, J.M. Revealing the impacts of transboundary pollution on $\text{PM}_{2.5}$ -related deaths in China. *Environ. Int.* **2020**, *134*, 105323. [[CrossRef](#)]
12. Li, X.L.; Hu, X.M.; Shi, S.Y.; Shen, L.D.; Luan, L.; Ma, Y.J. Spatiotemporal variations and regional transport of air pollutants in two urban agglomerations in northeast China plain. *Chin. Geogr. Sci.* **2019**, *29*, 917–933. [[CrossRef](#)]
13. Nan, Y.; Zhang, Q.Q.; Zhang, B.H. Analysis on the influencing factors of long-term change of grid $\text{PM}_{2.5}$ in typical regions of China based on gam model. *Environ. Sci.* **2020**, *41*, 499–509.
14. Chen, W.W.; Zhang, S.C.; Tong, Q.S.; Zhang, X.L.; Zhao, H.M.; Ma, S.Q.; Xiu, A.J.; He, Y.X. Regional characteristics and causes of haze events in Northeast China. *Chin. Geogr. Sci.* **2018**, *28*, 836–850. [[CrossRef](#)]
15. Gao, C.; Xiu, A.; Zhang, X.; Chen, W.; Liu, Y.; Zhao, H.; Zhang, S. Spatiotemporal characteristics of ozone pollution and policy implications in Northeast China. *Atmos. Pollut. Res.* **2020**, *11*, 357–369. [[CrossRef](#)]

16. Liang, Z.H.; Ju, T.Z.; Dong, H.P.; Geng, T.Y.; Duan, J.L.; Huang, R.R. Study on the variation characteristics of tropospheric ozone in Northeast China. *Environ. Monit. Assess.* **2021**, *193*, 282. [[CrossRef](#)] [[PubMed](#)]
17. Wang, H.; Ding, K.; Huang, X.; Wang, W.; Ding, A. Insight into ozone profile climatology over northeast China from aircraft measurement and numerical simulation. *Sci. Total Environ.* **2021**, *785*, 147308. [[CrossRef](#)]
18. Luo, M.; Ji, Y.Y.; Ren, Y.Q.; Gao, F.H.; Zhang, H.; Zhang, L.H.; Yu, Y.Q.; Li, H. Characteristics and health risk assessment of PM_{2.5}-Bound PAHs during heavy air pollution episodes in winter in urban area of Beijing, China. *Atmosphere* **2021**, *12*, 323. [[CrossRef](#)]
19. Li, B.; Shi, X.F.; Liu, Y.P.; Lu, L.; Wang, G.L.; Thapa, S.; Sun, X.Z.; Fu, D.L.; Wang, K.; Qi, H. Long-term characteristics of criteria air pollutants in megacities of Harbin-Changchun megalopolis, Northeast China: Spatiotemporal variations, source analysis, and meteorological effects. *Environ. Pollut.* **2020**, *267*, 10. [[CrossRef](#)] [[PubMed](#)]
20. Dai, H.B.; Zhu, J.; Liao, H.; Li, J.D.; Liang, M.X.; Yang, Y.; Yue, X. Co-occurrence of ozone and PM_{2.5} pollution in the Yangtze River Delta over 2013–2019: Spatiotemporal distribution and meteorological conditions. *Atmos. Res.* **2021**, *249*, 9. [[CrossRef](#)]
21. Wang, Y.Q.; Zhang, X.Y.; Draxler, R.R. TrajStat: GIS-based software that uses various trajectory statistical analysis methods to identify potential sources from long-term air pollution measurement data. *Environ. Model. Softw.* **2009**, *24*, 938–939. [[CrossRef](#)]
22. Wang, X.Q.; Zhang, T.S.; Xiang, Y.; Lv, L.H.; Fan, G.Q.; Ou, J.P. Investigation of atmospheric ozone during summer and autumn in Guangdong Province with a lidar network. *Sci. Total Environ.* **2021**, *751*, 141740. [[CrossRef](#)]
23. Stein, A.F.; Draxler, R.R.; Rolph, G.D.; Stunder, B.J.B.; Cohen, M.D.; Ngan, F. NOAA's hysplit atmospheric transport and dispersion modeling system. *bull. Amer. Meteorol. Soc.* **2015**, *96*, 2059–2077. [[CrossRef](#)]
24. Stohl, A.; Forster, C.; Frank, A.; Seibert, P.; Wotawa, G. Technical note: The Lagrangian particle dispersion model FLEXPART version 6.2. *Atmos. Chem. Phys.* **2005**, *5*, 2461–2474. [[CrossRef](#)]
25. Zhang, Y.R.; Zhang, H.L.; Deng, J.J.; Du, W.J.; Hong, Y.W.; Xu, L.L.; Qiu, Y.Q.; Hong, Z.Y.; Wu, X.; Ma, Q.L.; et al. Source regions and transport pathways of PM_{2.5} at a regional background site in East China. *Atmos. Environ.* **2017**, *167*, 202–211. [[CrossRef](#)]
26. Cesari, R.; Paradisi, P.; Allegrini, P. Source identification by a statistical analysis of backward trajectories based on peak pollution events. *Int. J. Environ. Pollut.* **2014**, *55*, 94–103. [[CrossRef](#)]
27. Sparks, D.N. Euclidean cluster analysis. *R. Stat. Soc. Ser. C Appl. Stat.* **1973**, *22*, 126–130. [[CrossRef](#)]
28. Hong, Q.Q.; Liu, C.; Hu, Q.H.; Xing, C.Z.; Tan, W.; Liu, H.R.; Huang, Y.; Zhu, Y.; Zhang, J.S.; Geng, T.Z.; et al. Evolution of the vertical structure of air pollutants during winter heavy pollution episodes: The role of regional transport and potential sources. *Atmos. Res.* **2019**, *228*, 206–222. [[CrossRef](#)]
29. Zhang, Z.Y.; Wong, M.S.; Lee, K.H. Estimation of potential source regions of PM_{2.5} in Beijing using backward trajectories. *Atmos. Pollut. Res.* **2015**, *6*, 173–177. [[CrossRef](#)]
30. Ashbaugh, L.L.; Malm, W.C.; Sadeh, W.Z. A residence time probability analysis of sulfur concentrations at grand Canyon National Park. *Atmos. Environ.* **1985**, *19*, 1263–1270. [[CrossRef](#)]
31. Hsu, Y.K.; Holsen, T.M.; Hopke, P.K. Locating and quantifying PCB sources in Chicago: Receptor modeling and field sampling. *Environ. Sci. Technol.* **2003**, *37*, 681–690. [[CrossRef](#)] [[PubMed](#)]
32. Wang, Y.Q.; Zhang, X.Y.; Arimoto, R. The contribution from distant dust sources to the atmospheric particulate matter loadings at XiAn, China during spring. *Sci. Total Environ.* **2006**, *368*, 875–883. [[CrossRef](#)]
33. Jeong, U.; Kim, J.; Lee, H.; Jung, J.; Kim, Y.J.; Song, C.H.; Koo, J.H. Estimation of the contributions of long range transported aerosol in East Asia to carbonaceous aerosol and PM concentrations in Seoul, Korea using highly time resolved measurements: A PSCF model approach. *J. Environ. Monit.* **2011**, *13*, 1905–1918. [[CrossRef](#)]
34. Kabashnikov, V.P.; Chaikovskiy, A.P.; Kucsera, T.L.; Metelskaya, N.S. Estimated accuracy of three common trajectory statistical methods. *Atmos. Environ.* **2011**, *45*, 5425–5430. [[CrossRef](#)]
35. Dimitriou, K. The dependence of PM size distribution from meteorology and local-regional contributions, in Valencia (Spain)—A CWT model approach. *Aerosol Air Qual. Res.* **2015**, *15*, 1979–1989. [[CrossRef](#)]
36. Zhang, Y.; Wang, W.; Wu, S.Y.; Wang, K.; Minoura, H.; Wang, Z.F. Impacts of updated emission inventories on source apportionment of fine particle and ozone over the southeastern US. *Atmos. Environ.* **2014**, *88*, 133–154. [[CrossRef](#)]
37. Otero, N.; Sillmann, J.; Schnell, J.L.; Rust, H.W.; Butler, T. Synoptic and meteorological drivers of extreme ozone concentrations over Europe. *Environ. Res. Lett.* **2016**, *11*, 13. [[CrossRef](#)]
38. Fan, H.; Zhao, C.F.; Yang, Y.K.; Yang, X.C. Spatio-temporal variations of the PM_{2.5}/PM₁₀ ratios and its application to air pollution type classification in China. *Front. Environ. Sci.* **2021**, *9*, 281. [[CrossRef](#)]
39. Pan, L.; Xu, J.M.; Tie, X.X.; Mao, X.Q.; Gao, W.; Chang, L.Y. Long-term measurements of planetary boundary layer height and interactions with PM_{2.5} in Shanghai, China. *Atmos. Pollut. Res.* **2019**, *10*, 989–996. [[CrossRef](#)]
40. Chen, Z.; Chen, D.; Zhao, C.; Kwan, M.P.; Cai, J.; Zhuang, Y.; Zhao, B.; Wang, X.; Chen, B.; Yang, J.; et al. Influence of meteorological conditions on PM_{2.5} concentrations across China: A review of methodology and mechanism. *Environ. Int.* **2020**, *139*, 105558. [[CrossRef](#)] [[PubMed](#)]
41. Zhao, H.; Che, H.; Zhang, X.; Ma, Y.; Wang, Y.; Wang, X.; Liu, C.; Hou, B.; Che, H. Aerosol optical properties over urban and industrial region of Northeast China by using ground-based sun-photometer measurement. *Atmos. Environ.* **2013**, *75*, 270–278. [[CrossRef](#)]

42. Zhao, H.; Gui, K.; Ma, Y.; Wang, Y.; Wang, Y.; Wang, H.; Zheng, Y.; Li, L.; Zhang, L.; Che, H.; et al. Climatological variations in aerosol optical depth and aerosol type identification in Liaoning of Northeast China based on MODIS data from 2002 to 2019. *Sci. Total Environ.* **2021**, *781*, 146810. [[CrossRef](#)]
43. Xu, Z.; Huang, X.; Nie, W.; Chi, X.; Xu, Z.; Zheng, L.; Sun, P.; Ding, A. Influence of synoptic condition and holiday effects on VOCs and ozone production in the Yangtze River Delta region, China. *Atmos. Environ.* **2017**, *168*, 112–124. [[CrossRef](#)]
44. Chen, J.; Shen, H.; Li, T.; Peng, X.; Cheng, H.; Ma, A.C. Temporal and spatial features of the correlation between PM_{2.5} and O₃ concentrations in China. *Int. J. Environ. Res. Public Health* **2019**, *16*, 4824. [[CrossRef](#)] [[PubMed](#)]
45. Tui, Y.; Qiu, J.; Wang, J.; Fang, C. Analysis of spatio-temporal variation characteristics of main air pollutants in Shijiazhuang city. *Sustainability* **2021**, *13*, 941. [[CrossRef](#)]
46. Chan, K.L.; Wang, S.S.; Liu, C.; Zhou, B.; Wenig, M.O.; Saiz-Lopez, A. On the summertime air quality and related photochemical processes in the megacity Shanghai, China. *Sci. Total Environ.* **2017**, *580*, 974–983. [[CrossRef](#)]
47. Qian, Y.; Xu, B.; Xia, L.J.; Chen, Y.L.; Deng, L.C.; Wang, H.; Zhang, G. Characteristics of ozone pollution and relationships with meteorological factors in Jiangxi province. *Environ. Sci.* **2021**, *42*, 2190–2201. [[CrossRef](#)]
48. Huang, D.; Li, Q.L.; Wang, X.X.; Li, G.X.; Sun, L.Q.; He, B.; Zhang, L.; Zhang, C.S. Characteristics and trends of ambient ozone and nitrogen oxides at urban, suburban, and rural sites from 2011 to 2017 in Shenzhen, China. *Sustainability* **2018**, *10*, 530. [[CrossRef](#)]
49. Wang, T.; Xue, L.K.; Brimblecombe, P.; Lam, Y.F.; Li, L.; Zhang, L. Ozone pollution in China: A review of concentrations, meteorological influences, chemical precursors, and effects. *Sci. Total Environ.* **2017**, *575*, 1582–1596. [[CrossRef](#)]
50. Gu, Y.; Liu, B.S.; Li, Y.F.; Zhang, Y.F.; Bi, X.H.; Wu, J.H.; Song, C.B.; Dai, Q.L.; Han, Y.; Ren, G.; et al. Multi-scale volatile organic compound (VOC) source apportionment in Tianjin, China, using a receptor model coupled with 1-hr resolution data. *Environ. Pollut.* **2020**, *265*, 23. [[CrossRef](#)]
51. Li, C.; Liu, Y.; Cheng, B.; Zhang, Y.; Liu, X.; Qu, Y.; An, J.; Kong, L.; Zhang, Y.; Zhang, C.; et al. A comprehensive investigation on volatile organic compounds (VOCs) in 2018 in Beijing, China: Characteristics, sources and behaviours in response to O₃ formation. *Sci. Total Environ.* **2022**, *806*, 150247. [[CrossRef](#)] [[PubMed](#)]
52. Liu, H.; Zhang, M.; Han, X. A review of surface ozone source apportionment in China. *Atmos. Ocean. Sci. Lett.* **2020**, *13*, 470–484. [[CrossRef](#)]
53. Zhang, H.; Qiu, Z.; Sun, D.; Wang, S.; He, Y. Seasonal and interannual variability of satellite-derived chlorophyll-a (2000–2012) in the Bohai Sea, China. *Remote Sens.* **2017**, *9*, 582. [[CrossRef](#)]
54. Yin, S.; Wang, X.; Zhang, X.; Zhang, Z.; Xiao, Y.; Tani, H.; Sun, Z. Exploring the effects of crop residue burning on local haze pollution in Northeast China using ground and satellite data. *Atmos. Environ.* **2019**, *199*, 189–201. [[CrossRef](#)]